

METHODOLOGY

Open Access



Hyperspectral lidar for monitoring high-resolution activity patterns of African stingless bee species

Hampus Månefjord^{1*}, A. Andrew Huzortey², Rabbi Boateng², Y. Adolphe Gbogbo³, A. S. Doria Yamoá³, Jérémie T. Zoueu³, Peter K. Kwapong⁶, Benjamin Anderson² and Mikkel Brydegaard^{1,4,5,7}

Abstract

Background Stingless bees are vital pollinators and honey producers in the tropics. Research on stingless bees is generally underrepresented compared to the western honeybees, and while stingless bee studies from some regions are reported, there is a particular lack of reports on the species endemic to Sub-Saharan Africa. Since conventional entomological methods such as mark-recapture and radar harmonic tags suffer from limited observation counts and amount to a significant payload, fluorescent powder tagging offers a promising alternative to understanding their behavior. We deploy a hyperspectral fluorescence lidar monitors a 25-mm-wide transect in front of the hives.

Results During a 1 day study at the International Stingless Bee Center, near Kakum National Park, Ghana, 17,862 insects were observed with the lidar, of which 7520 were tagged with fluorescent dyes. Approximately half of the bees from the selected hives were successfully tagged, with an estimated misclassification of 1%. According to our limited data, the observed species, *Meliponula bocandei* and the *Dactylurina staudingeri* exhibited different activity patterns. *D. staudingeri* displayed a half-hour longer active day, with clear crepuscular activity peaks. In contrast, *M. bocandei* activity was diurnal, with less pronounced crepuscular peaks.

Conclusions We demonstrate how hyperspectral fluorescence lidar can monitor powder-tagged insects throughout the day. The monitored species revealed distinct activity patterns over the day. Our findings highlight the potential of this technology as a valuable tool for understanding insect behavior and environmental preferences of species, in situ, which could potentially give clues of response to climate changes of these critical species.

Keywords Scheimpflug lidar, Fluorescence lidar, Hyperspectral lidar, Remote sensing, Pollination, Stingless bees, *Meliponula bocandei*, *Dactylurina staudingeri*, 3D-printed instrumentation, Low-cost instrumentation, Powder tagging, Marking

*Correspondence:

Hampus Månefjord

hampus.manefjord@forbrf.lth.se

Full list of author information is available at the end of the article



© The Author(s) 2024. **Open Access** This article is licensed under a Creative Commons Attribution 4.0 International License, which permits use, sharing, adaptation, distribution and reproduction in any medium or format, as long as you give appropriate credit to the original author(s) and the source, provide a link to the Creative Commons licence, and indicate if changes were made. The images or other third party material in this article are included in the article's Creative Commons licence, unless indicated otherwise in a credit line to the material. If material is not included in the article's Creative Commons licence and your intended use is not permitted by statutory regulation or exceeds the permitted use, you will need to obtain permission directly from the copyright holder. To view a copy of this licence, visit <http://creativecommons.org/licenses/by/4.0/>. The Creative Commons Public Domain Dedication waiver (<http://creativecommons.org/publicdomain/zero/1.0/>) applies to the data made available in this article, unless otherwise stated in a credit line to the data.

Introduction

Pollinators, particularly bees, play an indispensable role in supporting wild ecosystems [1] and agricultural production [2]. Honeybees often dominate the discourse on pollination, and their decline is covered in contemporary studies [3, 4]. However, in tropical and subtropical regions worldwide, the stingless bees comprise a majority of all eusocial bees, both in abundance and diversity [5, 6]. Stingless bees contribute to ecosystem biodiversity and bolster food security across Latin and South America, Asia, and Africa by pollinating a diverse range of crops [5, 7, 8]. They face alarming declines worldwide [9–11], and as a response, there are global interest in preservation as indicated by governmental and private initiatives [12]. Beyond their role in pollination, stingless bees, through meliponiculture (raising stingless bees), yield products such as honey, cerumen, propolis, and pollen. These products have significant economic and cultural value across societies [9, 13–16]. Despite their global relevance, there remains a notable research gap concerning stingless bees, particularly in Africa [17].

Understanding the activity patterns of these bees is crucial for discerning their distinct foraging strategies, relevant to tasks such as pollination [18], honey production [19], and social cohesion within wild bee communities [20]. Comparative studies highlight that foraging strategies diverge among bee species. In Brazil, the stingless bee species *Melipona subnitida* was observed to decrease their pollen foraging round-trip durations during the hottest hours of the day [21]. In Australia, the species *Trigona carbonaria* Smith's daily activity period was found to be longer during the warmer months [22]. In Costa Rica, *Melipona fasciata*, *M. beecheii*, and *M.*

favosa had longer daily foraging periods than *Tetragonisca angustula* [23]. Such environmental preferences could indicate the species' responses to upcoming climate changes. However, monitoring with high temporal resolution on multiple individuals is typically hindered by the lack of time-resolved data from conventional research methodologies [24, 25]. Furthermore, to our knowledge, no studies have detailed the daily activity pattern of the endemic African species *Meliponula bocandei* and *Dactylurina staudingeri*. Both species are honey producing eusocial bees that thrive across Ghana's diverse ecological zones [26, 27]. *M. bocandei* typically nests in cavities featuring narrow entrance slits, while *D. staudingeri* constructs exposed nests on tree branches with multiple entrances [28]. These species play a crucial role in pollinating a variety of crops, including coconut, citrus, mango, cashew, and shea butter, contributing significantly to agricultural biodiversity [29].

Insect behavior analysis involves a wide range of techniques (see Table 1 for an overview). While methods like manual trapping and counting [24] provide foundational data, they can be time consuming and lack fine-scale resolution. Non-tagging techniques such as image-based tracking [30–33] and digital holography [34] offer insights but may be limited by frame rates and processing demands. Hive entrance monitoring through visual observations and automated video tracking [35, 36], or hive sensors measuring weight, temperature, or vibrations [37] provide robust activity monitoring, but typically focus on the hives or their immediate vicinity. Radar and lidar show great potential for monitoring insect migration at high altitudes [38–40] but are typically not applicable for foraging bees close to canopies. Further,

Table 1 A comparison of different techniques for bee monitoring

Technique	Strengths	Weaknesses	Best use cases
Visual observation	Low cost, no setup	Labor-intensive, limited specificity	Insect abundance studies, behavioral/interaction studies
Traps	Species-specific, often low cost	Often biased, poor spatial and temporal resolutions	Species-specific abundance estimation
Hive sensors	High temporal resolution, low maintenance	Indirect measure, no individual tracking	Long-term colony monitoring
Video tracking	High spatial and temporal resolution, 3D tracking, low maintenance	Limited to specific observation area, needs data processing	Long-term and detailed movement tracking near hives
Mark-recapture	Can track individuals, movement patterns	Labor-intensive, may disturb behavior, specificity often relies on field identification	Population estimates, behavioral studies
Radar/lidar	Long range, high spatial and temporal resolution	High cost, resolution limitations for small insects, limited specificity	Large-scale migration, large-range dispersal patterns
Fluorescence-tagged lidar	Can track individuals or specific hives, high spatial and temporal resolution, long range	Requires specialized instrument and initial alignment. Needs data processing	High temporal and spatial resolution monitoring of selected hives/individuals

their ability to discriminate between species or individuals without additional tagging is limited [41, 42].

Tagging introduces specificity to entomological studies. Marking has been used for detailed analysis of insect lifespans [43], population densities [44], and dispersal patterns [45]. However, the efficacy of these tags varies. For instance, radio- and harmonic tags [46–48] are mainly used for tracing individual insects for long distances, and the payload weight can influence their behavior [49]. Combining fluorescence tagging with lidar was suggested decades ago [50], but had early challenges with observation counts and low signal strength [51]. Recent advancements include passive solar-induced fluorescence imaging. This method employs quantum dots as markers and harnesses the short-wave infrared (SWIR) solar absorption lines. However, its operation is confined to daytime hours and can be influenced by prevailing weather conditions [32]. In contrast, our group has introduced the active laser-induced fluorescence lidar [52], with no such limitations.

In this study, we used fluorescent tagging in combination with a novel hyperspectral lidar to investigate the activity patterns of the African stingless bee species *M. bocandei* and *D. staudingeri*. We aim to assess the performance of this method for entomological monitoring by a comparative study of two species of stingless bees in Ghana.

Materials and methods

Experiment

This study was conducted at the International Stingless Bee Center (ISBC) near Kakum National Park [53, 54], Ghana (5°20′28.4″N, 1°22′39.4″W) on 17th March 2022. The time of day is presented in solar time, with sunrise at 5:58 AM (91°E) and sunset at 6:03 PM (269°W). Temperature ranged from 26 °C to 32 °C, there was no rain, clear skies, and wind was below 3 m/s. Beehives of species *Meliponula bocandei* (*M. bocandei*),

Dactylurina staudingeri (*D. staudingeri*), *Hypotrigona*, and *Meliponula ferruginea* were present on-site. The entrances of two hives were dusted with distinct fluorescent dyes (UV Holi powder, PaintGlow, UK): *M. bocandei* (green color) and *D. staudingeri* (red color), such that the bees leaving the entrance were auto-tagged. Dye was reapplied to the entrances with 2-h intervals. These colonies have been maintained at the ISBC for over a decade, and were originally collected from the wild [53]. There was no possibility to alter the positions of hives at the ISBC; hence, measurements were carried out with unmarked hives in the vicinity of the transect.

A hyperspectral fluorescence lidar was used to monitor a 25-mm-wide transect starting 5.8 m from the lidar and terminated on a neoprene board 23 m from the lidar. The lidar beam passed ~15 cm in front of both entrances of the tagged beehives located at 11 m and 17 m from the lidar (see Fig. 1). All other hives entrances were at distances >50 cm from the transect. The lidar was powered by a diesel generator, allowing for 24 h of uninterrupted measurement, see Fig. 1a, b for an overview of the lidar transect and detailed lidar components.

Instrument

The hyperspectral lidar, inspired by [55, 56], was built at the Laser and Fibre Optics Centre (LAFOC) at the University of Cape Coast (UCC) in Ghana. The design and specifications were identical to those used in prior remote sensing fluorescence studies [52, 57, 58], with detailed parts, calibration information, and assembly instructions available in [52]. The lidar featured a 1 W, 405 nm laser diode expanded to Ø25 mm with a collimating lens, followed by a folding mirror for alignment (Fig. 1b). The illuminated air was imaged onto a 200 µm slit by a Ø75 mm achromat by utilizing the “Scheimpflug configuration” and the “hinge rule” [59]. The slit was subsequently imaged onto the broad side of a CMOS image chip (1920 × 1200 pixel, 12-bit), with

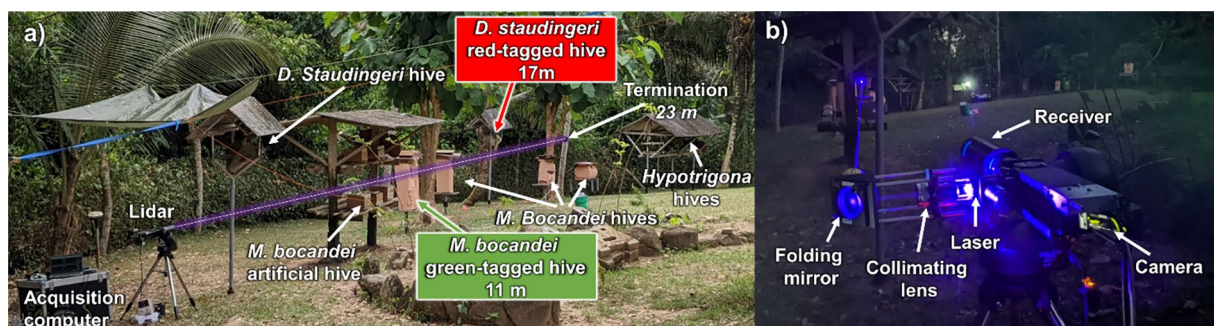


Fig. 1 Experimental setup **a** The lidar transect at the International Stingless bee center. The two tagged hives and all untagged hives in view are indicated. **b** Close-up photo of the lidar, highlighting major components

a range accuracy of 5%. A grating-based spectroscopic insert was positioned between the slit and the camera, providing spectral information in the other direction of the sensor. The spectral range spans approximately 390 nm to 810 nm and is resolved with 70 effective spectral bands. A lock-in detection method [52, 60] was employed for real-time ambient light subtraction, enabling daytime measurements up to 100 m range. The measurement geometry is limited to narrow line transect, which could be problematic for complex habitats. This technique implies that the laser is switched off and on for alternating exposures, making every other exposure contain signal and background, respectively.

Data pipeline

During the 24 h measurement period, 25,982 measurement files were accumulated, each file representing a 3D data cube of intensity values $I(x, y, n)$ in 12-bit. Here, $x \in \{1 \dots x_{chip}\}$, and $y \in \{1 \dots y_{chip}\}$ are the pixel numbers where $x_{chip} = 1920$ pixels and $y_{chip} = 1200$ pixels are the number of pixels on the (1920 × 1200 pixel) chip. Each file contains $n \in \{1 \dots 256\}$ exposures, taken consecutively with 7.73 ms exposure time. One file covers 2 s, and the temporal fill factor is 60% due to delays between recorded files.

Range calibration: the range was estimated using the Scheimpflug configuration through

$$r(x) = \ell_{BL} \cot \left(\Phi_{slant} + \frac{\Theta_{FoV} x}{x_{chip}} \right), \quad (1)$$

where $\ell_{BL} = 310$ mm is the length of the baseline, $\Phi_{slant} = 2^\circ$ is the slant angle, and $\Theta_{FoV} = 6^\circ$ is the angle between the optical axis and the beam expander, as discussed in [61–63]. The estimated range spanned from 5.8 m to 120 m.

Wavelength calibration: the wavelength $\lambda(x, y)$ was estimated through

$$\lambda(x, y) = \lambda_0 + \lambda_{span} \frac{y}{y_{chip}} + \delta_{fan} \frac{x}{x_{chip}} \frac{y}{y_{chip}} + \delta_{bend} \left(\frac{x}{x_{chip}} \right)^2, \quad (2)$$

where $\lambda_0 \approx 385$ nm is the starting wavelength and $\lambda_{span} \approx 440$ nm is the wavelength span. The small coefficients, δ_{fan} and δ_{bend} , describe the undesired ‘keystone’ and ‘smile’ distortions [63, 64] that affect spectral registration at different ranges. The coefficients were determined using the known laser wavelength of the first and second diffraction orders at all ranges [52].

Background subtraction: lock-in detection was employed by switching the laser *on* and *off* for odd and even exposures. A background-subtracted signal was obtained by linear interpolation [65].

The above calibration procedure allowed each data cube $I(x, y, n)$ to be analyzed and visualized with its range, wavelength, and time information represented in SI units, $I(r, \lambda, t)$. One example data file is visualized in Fig. 2a in a 3D plot. In this data file the termination board is visible, and five insects were observed, two of which were powder tagged. The termination echo remains static over time at the 23 m range. The wavelength response is the same as the output laser wavelength, a so-called elastic signal at $\lambda_{elastic} = 405$ nm. However, the second diffraction order of the elastic laser wavelength is also mapped at $\lambda_{2nd} = 810$ nm. The termination echo appears as two horizontal lines, one for each diffraction order. The five insect observations manifest as elastic signals of first and second diffraction order. The fluorescence-tagged insects (highlighted in red and green in Fig. 2a) exhibit, in addition to the elastic signals, a green and a red fluorescence peak, respectively.

An insect detection scheme was established to find all insect observations. First, a region of interest in the range domain was defined as $r \in [5.8 \text{ m} \dots 21 \text{ m}]$ to exclude the termination echo from further processing. Then, a signal-to-noise ratio $SNR(r, t)$ was determined for each remaining time-range element by a spectral differentiation method:

$$SNR_{elastic}(r, t) = \frac{|I(r, \lambda_{elastic}, t)|_{\max} - |I(r, \lambda_{noise}, t)|_{\text{median}}}{|I(r, \lambda_{noise}, t)|_{\max} - |I(r, \lambda_{noise}, t)|_{\text{median}}}, \quad (3)$$

where the maximum and median intensity norms were evaluated at the elastic wavelength $\lambda_{elastic}$ and in a noise region surrounding the elastic wavelength, $\lambda_{noise} = [390 \text{ nm} \dots 400 \text{ nm}, 410 \text{ nm} \dots 425 \text{ nm}]$. We defined another SNR measure for the second-order diffracted light,

$$SNR_{2nd}(r, t) = \frac{|I(r, \lambda_{2nd}, t)|_{\max} - |I(r, \lambda_{noise2}, t)|_{\text{median}}}{|I(r, \lambda_{noise2}, t)|_{\max} - |I(r, \lambda_{noise2}, t)|_{\text{median}}}, \quad (4)$$

where $\lambda_{noise2} = [790 \text{ nm} \dots 805 \text{ nm}, 815 \text{ nm} \dots 825 \text{ nm}]$. The minimum between $SNR_{elastic}$ and SNR_{2nd} for each range–time pixel formed $SNR(r, t)$, which is displayed for the example data file in Fig. 2b. Defining the final $SNR(r, t)$ as the minimum of both the first- and second-order SNR reduces misclassification due to noise at the $\lambda_{elastic}$ region or λ_{2nd} , respectively. This process is illustrated in Fig. 2c, where the $SNR_{elastic} = 93$ and $SNR_{2nd} = 36$, yielding an SNR of 36 for the insect observation.

The $SNR(r, t)$ was compared to a threshold value SNR_{thres} producing a binary mask image $B(t, r) = SNR(r, t) > SNR_{thres}$, resulting in $B(t, r) = 1$ for all (r, t) combinations that include an insect observation and $B(t, r) = 0$ otherwise. The binary image was then dilated to connect multiple exposures of the same insect. Five observations were found in the example file evaluated

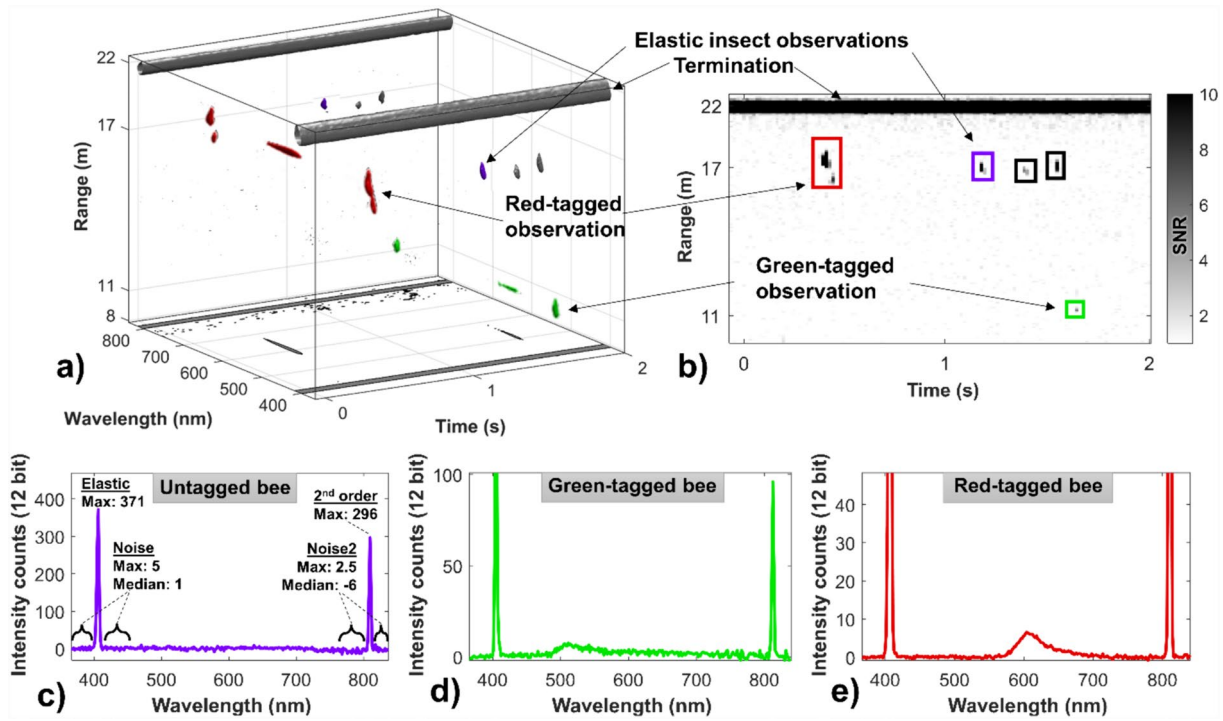


Fig. 2 Data processing of a measurement file with insect observations. **a** Intensity values $I(r, \lambda, t)$ of a measurement file containing five insect observations and the termination echo. Three selected insect observations are highlighted in different colors, an untagged—in violet, a green-tagged—in green, and a red-tagged—in red. The 3D signals are also projected in black to the wavelength–time plane at the bottom of the plot. **b** The signal-to-noise ratio $SNR(t, r)$ of each range–time element of the measurement file. The selected insects’ spectra are in their respective colors in **(c)**, **(d)**, and **(e)**. The values used to calculate the SNR in Eq. 1 and Eq. 2 are displayed in **(c)**

in Fig. 2: three are purely elastic, one shows green fluorescence, and one shows red fluorescence. Three of the observations are highlighted in color in Fig. 2a,b; the corresponding spectra of the highlighted observations are found in Fig. 2c, e.

Metadata were saved for each extracted insect observation, and these data include the time and range information and quantification of how much elastic, green fluorescent, and red fluorescent light is detected. The quantification was accomplished by averaging the intensities of the corresponding spectral, range Δr , and time Δt regions of the observation,

$$\begin{aligned}
 I_{\text{elastic}} &= \frac{1}{\Delta r \Delta t} \sum_{r=\Delta r} \sum_{\lambda=\lambda_{\text{elastic}}} \sum_{t=\Delta t} I(r, \lambda, t), I_{\text{green}} \\
 &= \frac{1}{\Delta r \Delta \lambda_{\text{green}} \Delta t} \sum_{r=\Delta r} \sum_{\lambda=\Delta \lambda_{\text{green}}} \sum_{t=\Delta t} I(r, \lambda, t), I_{\text{red}} \\
 &= \frac{1}{\Delta r \Delta \lambda_{\text{red}} \Delta t} \sum_{r=\Delta r} \sum_{\lambda=\Delta \lambda_{\text{green}}} \sum_{t=\Delta t} I(r, \lambda, t).
 \end{aligned}
 \tag{5}$$

The spectral regions $\Delta \lambda_{\text{green}} = [490 \text{ nm} \dots 530 \text{ nm}]$ and $\Delta \lambda_{\text{red}} = [580 \text{ nm} \dots 630 \text{ nm}]$ correspond to the fluorescent

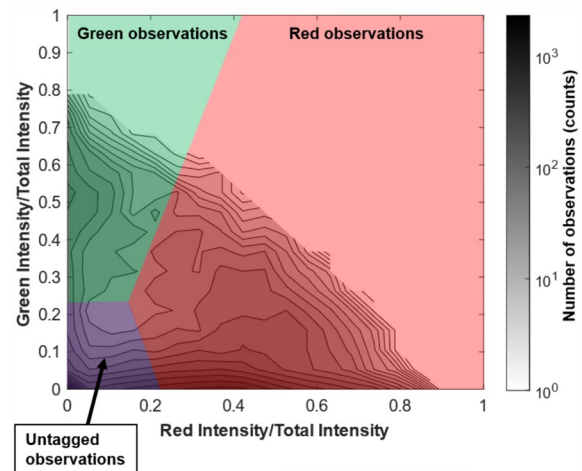


Fig. 3 Observation classification. A histogram of values of \hat{I}_{green} and \hat{I}_{red} for all observations. The threshold values for classifying an observation as untagged, green, or red fluorescent are visualized by colored regions in the contour plot

regions of the green and red powder, respectively. Normalized intensities,

$$\begin{aligned} \hat{I}_{green} &= \frac{I_{green}}{I_{elastic} + I_{green} + I_{red}}, \\ \hat{I}_{red} &= \frac{I_{red}}{I_{elastic} + I_{green} + I_{red}}, \end{aligned} \tag{6}$$

from all observations are shown as a 2D histogram contour plot in Fig. 3. The observations were classified as untagged, green, or red fluorescent based on the values of \hat{I}_{green} and \hat{I}_{red} . The classification thresholds are set by identifying the saddle points within the data in Fig. 3.

Analyzing all measurement files gave statistics on the SNR in the time–range pixels. A histogram of the SNR values is shown in Fig. 4a, where the insect observation and noise values follow two distinct lines in the plot. An SNR threshold value SNR_{thres} can be set to a value that excludes most of the noise, as discussed in [65]. The mean, μ , and the standard deviation, σ , of the background subtracted observation spectra and the background from all observations are shown in Fig. 4b.

The described data pipeline effectively detects insects by differentiating the spectral response around the emitted wavelength, both at the sensor’s first and second diffraction orders. Through extensive statistical analysis, a robust threshold is set. The observations are classified

with a minimalistic scheme integrating intensity in different spectral regions.

Results

The stingless bee activity during the 24 h measurement period is shown in Fig. 5. A total of 17,862 insects were observed with the lidar, with 7520 (42%) identified as tagged with fluorescent dye. This observation count equates to an average of ~1 insect per minute per meter throughout the day. However, this number was at its peak of ~50 insects per minute per meter during the morning rush hour (7:45–8:15).

The observations are categorized into green-tagged (*M. bocandei*), red-tagged (*D. staudingeri*), and untagged, represented in a contour plot as green, red, and gray, respectively (see Fig. 5a). The observation density (counts per meter) and frequency (counts per minute) throughout the day are displayed in Fig. 5b and Fig. 5c. Most of the green-tagged observations are found at the 11 m mark during daylight, while red-tagged observations are mostly found at the 17 m mark. This pattern is consistent with the locations of the tagged hives at 11 and 17 m from the lidar and the diurnal behavior of stingless bees. Due to imperfect powder tagging yield, untagged observations also have activity peaks at these distances, although less pronounced.

The activity patterns in Fig. 5c differ between the two tagged species and the untagged ones. *D. staudingeri* were observed from 05:50 (8 min before sunrise) to 18:04 (1 min past sunset) with pronounced crepuscular activity peaks (8:00 and 16:30) and an activity minimum at 15:00. *M. bocandei* showed a 33-min shorter active day (06:12–17:53), with no morning peak but increased activity throughout the day, culminating in a peak at 16:30.

Table 2 defines four different regions of range and time of day. Different classifications of the observations are evaluated within the regions (see Fig. 5d). The tagging yield ranged from 42 to 46% in the first two regions. However, accounting for other insects likely found within the defined ranges (estimated to ~300 counts per meter), the tagging yield increased to 51% and 48%, respectively. The misclassification between red and green observations is estimated to ~1% using the assumption that there should be no increased activity at the entrance of the other species. This implies that ~1% of the bees that were classified as red-tagged, was in reality green-tagged, and vice versa. Far from the hives 4–6% of the observations were tagged, and during nighttime, no tagged observations were recorded, underscoring the high reliability of the classification between elastic and fluorescent observations.

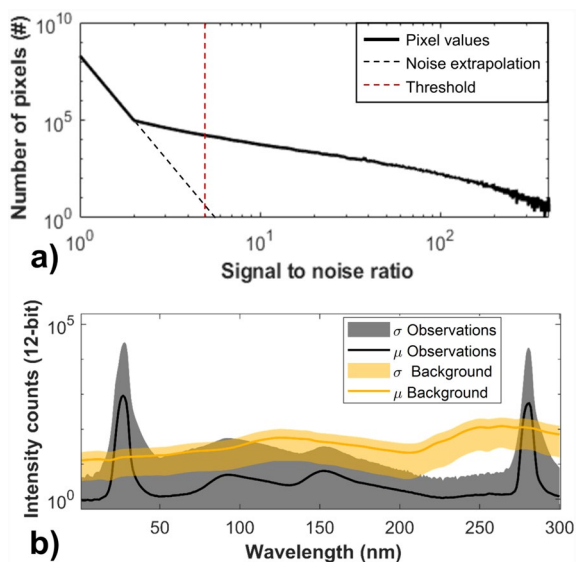


Fig. 4 Statistical analysis on all insect observations. **a** Log-log histogram of the SNR values of each time–range pixel in all measurement files during 24 h. An extrapolation of the noise and the selected threshold value are indicated in dashed lines. **b** The mean and standard deviation of the background subtracted spectra and the backgrounds of all insect observations

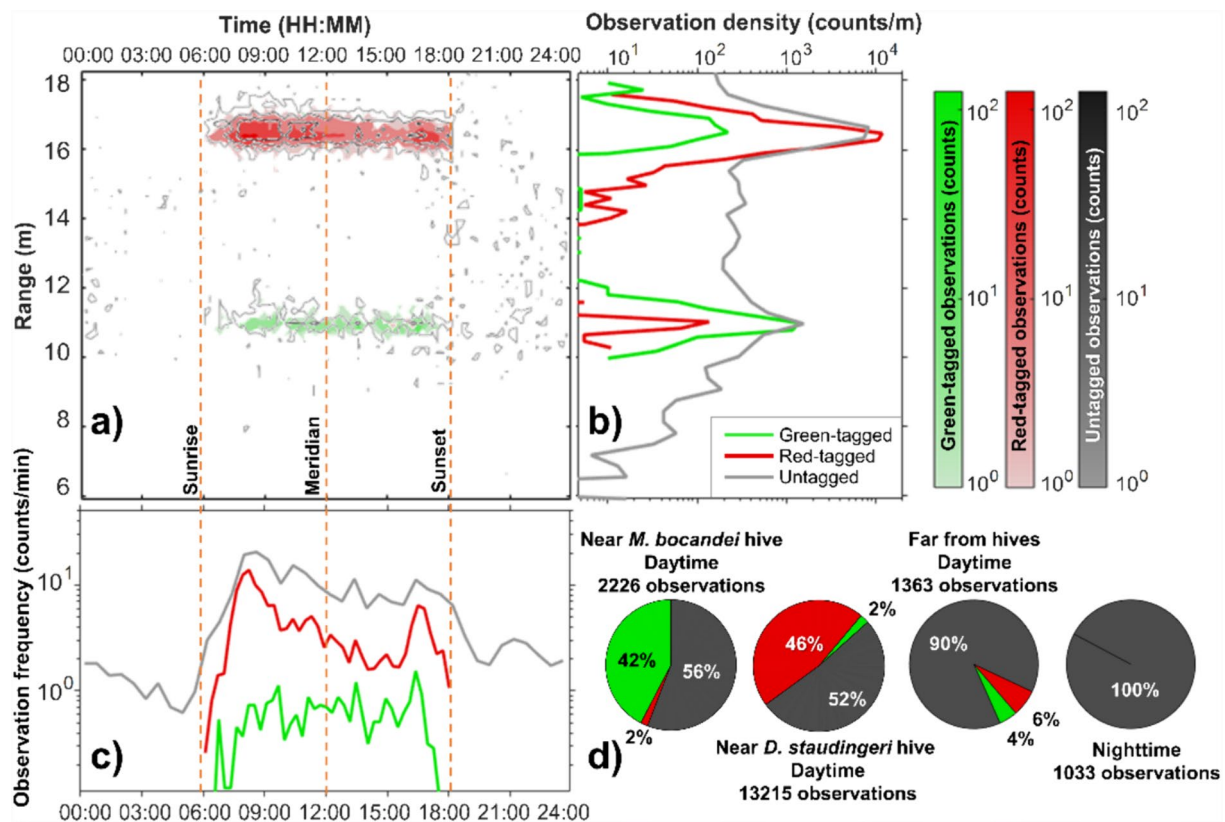


Fig. 5 Insect activity for 24 h. Green-tagged (*M. bocandei*), red-tagged (*D. staudingeri*), and untagged insect observations of the 24-h measurement are presented as **(a)** a contour plot over time of day and range. The sunrise (at 5:58), the meridian (at 12:00), and the sunset (at 18:03) are marked with dashed lines. **(b)** The observation density over the range in counts per meter. **(c)** The observation frequency over time of day in counts per minute. In **(d)**, the percentage of green-tagged, red-tagged, and untagged insect observations are shown in intervals defined in Table II, close to and far from the two tagged hives and for day and nighttime

Table 2 Defined ranges and time of day for the ‘intervals’

Interval name	Range (m)	Time of day (HH;MM)
Near <i>M. bocandei</i> hive daytime	10.5–11.85	05:50–18:04
Near <i>D. staudingeri</i> hive daytime	15.8–17.5	05:50–18:04
Far from hives daytime	5.8–10.5, 11.85–15.8, 17.5–21	05:50–18:04
Nighttime	5.8–21	18:05–05:49

The observations and analyses presented offer detailed insights into the activity patterns of the two tagged species and untagged insects.

Discussion

Common methods for insect behavior monitoring, such as visual observation, hive sensors, and video tracking, offer valuable insights but often face limitations in specificity, spatial range, or temporal resolution. The

hyperspectral lidar method presented here aims to address these challenges by providing high-resolution and species-specific tracking capabilities. Here, we discuss the specific advantages of this lidar technique and areas where it complements, rather than replaces, existing methodologies.

We employed a novel hyperspectral lidar with the capability to monitor insects’ activities throughout both day and night along a 23 m transect, in front of their hives. This system detected over 17,000 tagged and untagged insects and provided millisecond temporal and centimeter spatial resolutions. Indeed, the ability to remotely detect small insects relies on the high resolution in time, range, and wavelength with lock-in and differentiation methods. The second diffraction order is usually considered undesirable but is, in our case, utilized to increase the reliability of detections and for continuous wavelength calibration. Although the frame rate is sufficient for distinguishing single observations, systems with kilohertz sample rates can determine, e.g., flight speed [41] and wingbeat frequency [66].

Our methodology of powder tagging has been reported to have little effect on flight behavior [67] compared to bulkier radio transmitters [68]. The labor required for our approach is notably less than conventional counting methods, making it a promising tool for extensive studies.

One constraint inherent to lidar systems is their one-dimensional monitoring. Expanding to 2D or 3D tracking in future work could offer broader insights. This approach could be achieved by scanning or wobbling the beam [57, 58, 69]. Furthermore, our study's confined transect (~20 m) restricted our observations to free-flying insects in proximity to the hives. Future research might benefit from exploring longer-range observations. This focused data collection along the transect could be greatly enriched by combining it with visual observations or localized hive monitoring. Such integration would offer insights into flight trajectories, behaviors near the hive entrance, and confirmation of any species identification made by the lidar system.

Since this study is limited in terms of duration and number of hives monitored, we cannot discern to what degree the patterns are influenced by attributes specific to the measuring day and these specific colonies' sizes and microclimates. A more rigorous study with multiple tagged hives and a longer duration could be explored in the future. However, we resolve distinct activity patterns of the two endemic stingless bee species, which showcases the possibilities of this technology. The variations between the two species, with the smaller *D. staudingeri* exhibiting a more extended active day yet less active during the warmer hours compared to the larger *M. bocandei*, offer intriguing ecological insights. Previous literature has noted a heightened heat sensitivity in pollen-collecting stingless bees compared to their nectar-foraging counterparts [21]. While some studies suggest that African endemic stingless bees demonstrate a preference for pollen [70], others specifically identify *M. bocandei* as primarily nectar foragers [71]. Our findings, which indicate greater heat resilience in *M. bocandei*, align with this latter observation. In Scotland, the larger bumblebees were found to be more resistant than honeybees to harsh, *i.e.*, cold, weather conditions, leading to longer active days [72]. Although more research is needed to confirm our findings, our results propose that in the tropics the opposite could hold true, insects with larger body sizes could have shorter active days and more activity during the warmest hours.

Conclusions

Our deployment of a novel hyperspectral lidar provided insights into the behavior of over 17,000 tagged and untagged insects. Combining high temporal and

spatial resolutions, the technology offers substantial improvements over conventional entomological methods. Notably, the unique activity patterns of the endemic stingless bees, *D. staudingeri* and *M. bocandei*, were revealed, offering ecological implications. We hope that the observed distinctness in the activity patterns of these species will aid the establishment of conservation strategies for stingless bees. Our methodology emerges as a promising tool for further ecological studies, increasingly relevant due to impending challenges like climate change and insect decline.

Supplementary Information

The online version contains supplementary material available at <https://doi.org/10.1186/s40317-024-00372-3>.

Additional file 1.

Acknowledgements

The authors thank Samuel Nkrumah and all the International Stingless Bee Center staff for hosting us during the experiment. They thank the team at Laser and Fiber Optics Center (LAFOC) at the University of Cape Coast for hosting the workshop and all participants from African Spectral Imaging Network (AFSIN), including Moses Jojo Eghan, Peter Osei-Wusu Adueming, Jerry Opoku-Ansah, and Charles Lloyd Yeboah Amuah.

Author contributions

MB, BA, and JZ acquired the grants. PK owns and manages the International Stingless Bee Center. HM and MB designed the instrument. HM wrote the acquisition software and the analysis code, analyzed data, and produced graphical items. HM, AH, RB, AG, DY, MB, and BA constructed the lidar and carried out the experiment on-site. HM and PK drafted the manuscript. All authors contributed to the manuscript.

Funding

Open access funding provided by Lund University. This work was financed by a Uforsk Grant No. (2018-04073) from the Swedish Research Council to support realistic instrumentation and capacity building in low-income countries. The workshop and replication of the instrument were funded by the Swedish International Development Agency (SIDA) through the International Science Program (ISP, Uppsala) through a grant to the African Spectral Imaging Network (AFSIN).

Availability of data and materials

A processed version of the datasets used during the current study is available as supporting files, additional data can be made available from the corresponding author on request.

Declarations

Ethics approval and consent to participate

Not applicable.

Consent for publication

Not applicable.

Competing interests

Not applicable.

Author details

¹Department of Physics, Lund University, Sölvegatan 14, 223 62 Lund, Sweden. ²Laser and Fibre Optics Centre, Department of Physics, University of Cape Coast, Cape Coast, Ghana. ³Laboratoire d'Instrumentation, Image Et Spectroscopie, INP-HB, BP 1093 Yamoussoukro, Côte d'Ivoire.

⁴FaunaPhotonics APS, Støberigade 14, 2450 Copenhagen, SV, Denmark.

⁵Department of Biology, Lund University, Sölvegatan 35, 223 62 Lund, Sweden.

⁶International Stingless Bee Center, Department of Conservation Biology and Entomology, University of Cape Coast, Cape Coast, Ghana. ⁷Norsk Elektro Optikk AS, Prost Stabels Vei 22, N-2019 Skedsmokorset, Norway.

Received: 22 November 2023 Accepted: 13 May 2024

Published online: 29 May 2024

References

- Ollerton J. Pollinator diversity: distribution, ecological function, and conservation. *Annu Rev Ecol Evol Syst.* 2017;48:353–76.
- Klein A-M, et al. Importance of pollinators in changing landscapes for world crops. *Proc R Soc B Biol Sci.* 2007;274(1608):303–13.
- Potts SG, et al. Global pollinator declines: trends, impacts and drivers. *Trend Ecol Evol.* 2010;25(6):345–53.
- Potts SG, et al. Declines of managed honey bees and beekeepers in Europe. *J Apic Res.* 2010;49(1):15–22.
- Michener CD. The bees of the world. Baltimore: JHU press; 2000.
- Grüter C. Stingless bees. Cham: Springer International Publishing; 2020. p. 1182–6.
- Slaa EJ, et al. Stingless bees in applied pollination: practice and perspectives. *Apidologie.* 2006;37(2):293–315.
- Giannini TC, et al. The dependence of crops for pollinators and the economic value of pollination in Brazil. *J Econ Entomol.* 2015;108(3):849–57.
- Chuttong B, Chanbang Y, Burgett M. Meliponiculture: stingless bee beekeeping in Thailand. *Bee World.* 2014;91(2):41–5.
- Toledo-Hernández E, et al. The stingless bees (hymenoptera: apidae: meliponini): a review of the current threats to their survival. *Apidologie.* 2022;53(1):8.
- Tornyie F, Kwapong PK. Nesting ecology of stingless bees and potential threats to their survival within selected landscapes in the northern volta region of Ghana. *Afr J Ecol.* 2015;53(4):398–405.
- Cortopassi-Laurino M, et al. Global meliponiculture: challenges and opportunities. *Apidologie.* 2006;37(2):275–92.
- Souza, B., M. Lopes, and F. Pereira. Cultural aspects of meliponiculture. 2012.
- Vit P, Pedro SR, Roubik DW. Pot-pollen in stingless bee mellittology. Berlin: Springer; 2018.
- Vit P, Pedro SR, Roubik D. Pot-honey: a legacy of stingless bees. New York: Springer Science and Business Media; 2013.
- Kwapong PK, Illechie AA, Kusi R. Comparative antibacterial activity of stingless bee honey and standard antibiotics against common eye pathogens. Cape Coast: University of Cape Coast; 2014.
- Karikari A, Kwapong P. A survey of indigenous knowledge of stingless bees (Apidae: Meliponini) in the central region of Ghana. *J Ghana Sci Assoc.* 2007. <https://doi.org/10.4314/jgsa.v9i2.48073>.
- Herrera CM. Daily patterns of pollinator activity, differential pollinating effectiveness, and floral resource availability, in a summer-flowering mediterranean shrub. *Oikos.* 1990. <https://doi.org/10.2307/3545218>.
- Danner N, et al. Season and landscape composition affect pollen foraging distances and habitat use of honey bees. *Ecol Appl.* 2016;26(6):1920–9.
- Pope NS, Jha S. Seasonal food scarcity prompts long-distance foraging by a wild social bee. *Am Nat.* 2018;191(1):45–57.
- Maia-Silva C, et al. Don't stay out too long! thermal tolerance of the stingless bees *Melipona subnitida* decreases with increasing exposure time to elevated temperatures. *Apidologie.* 2021;52(1):218–29.
- Heard TA, Hendrikz JK. Factors influencing flight activity of colonies of the stingless bee *Trigona carbonaria* (hymenoptera, apidae). *Aust J Zool.* 1993;41(4):343–53.
- De Bruijn L, Sommeijer MJ. Colony foraging in different species of stingless bees (apidae, meliponinae) and the regulation of individual nectar foraging. *Insectes Soc.* 1997;44:35–47.
- Muirhead-Thompson, R. Trap responses of flying insects: the influence of trap design on capture efficiency. 2012.
- Baum KA, Wallen KE. Potential bias in pan trapping as a function of floral abundance. *J Kansas Entomol Soc.* 2011;84(2):155–9.
- Cockburn C, et al. Shelf-life and variances in antimicrobial properties of honey from *Meliponula bocandei* and *Meliponula ferruginea* in central Ghana. *J Young Investig.* 2013;25(1):10–4.
- Mogho, N.M.T., D. Wittmann, and T.F. Ambebe. Nest architecture of *Dactylurina Staudingeri* (Hymenoptera, Apidae, Meliponini) in cameroon. 2016.
- Roubik D. Niche preemption in tropical bee communities: a comparison of neotropical and malasian faunas. In: Roubik D, editor. Niche preemption in tropical bee communities: a comparison of neotropical and malasian faunas. Sapporo: Hokkaido University Press; 1990. p. 245–57.
- Eardley C, Kwapong P. Taxonomy as a tool for conservation of African stingless bees and their honey. In: Vit P, Pedro SRM, Roubik D, editors. Pot-honey a legacy of stingless bees. New York: Springer; 2013. p. 261.
- Bjerger K, Mann HM, Høye TT. Real-time insect tracking and monitoring with computer vision and deep learning. *Remote Sens Ecol Conserv.* 2022;8(3):315–27.
- Butail S, et al. Reconstructing the flight kinematics of swarming and mating in wild mosquitoes. *J R Soc Interfac.* 2012;9(75):2624–38.
- Walter T, et al. A new innovative real-time tracking method for flying insects applicable under natural conditions. *BMC Zool.* 2021;6:1–11.
- Dell AI, et al. Automated image-based tracking and its application in ecology. *Trend Ecol Evol.* 2014;29(7):417–28.
- Hall ML, et al. The application of digital holography for accurate three-dimensional localisation of mosquito-bednet interaction. *Light Adv Manuf.* 2022;3(1):e20.
- Chiron G, Gomez-Krämer P, Ménard M. Detecting and tracking honeybees in 3D at the beehive entrance using stereo vision. *EURASIP J Imag Video Process.* 2013;2013(1):1–17.
- O'Shea-Wheller TA, et al. Quantifying the impact of an invasive hornet on bumblebee colonies. *Commun Biol.* 2023;6(1):990.
- Meikle W, Holst N. Application of continuous monitoring of honeybee colonies. *Apidologie.* 2015;46:10–22.
- Hu G, et al. Mass seasonal bioflows of high-flying insect migrants. *Science.* 2016;354(6319):1584–7.
- Drake VA, Wang H. Ascent and descent rates of high-flying insect migrants determined with a non-coherent vertical-beam entomological radar. *Int J Remote Sens.* 2018. <https://doi.org/10.1080/01431161.2018.1519283>.
- Tauc MJ, et al. Field demonstration of a wing-beat modulation lidar for the 3D mapping of flying insects. *OSA Contin.* 2019;2(2):332–48.
- Li Y, et al. Insect flight velocity measurement with a CW near-IR Scheimpflug lidar system. *Opt Expr.* 2020;28(15):21891–902.
- Jansson S, et al. Real-time dispersal of malaria vectors in rural Africa monitored with lidar. *PLoS ONE.* 2020. <https://doi.org/10.1371/journal.pone.0247803>.
- Sielezniew M, Kostro-Ambroziak A, Kőrösi Á. Sexual differences in age-dependent survival and life span of adults in a natural butterfly population. *Sci Rep.* 2020;10(1):1–10.
- Torres-Vila LM, et al. Assessing mass trapping efficiency and population density of *Cerambyx welensii* küster by mark-recapture in dehesa open woodlands. *Eur J Forest Res.* 2012;131(4):1103–16.
- Kirkeby C, et al. Quantifying dispersal of European culicoides (diptera: ceratopogonidae) vectors between farms using a novel mark-release-recapture technique. *PLoS ONE.* 2013;8(4): e61269.
- Pasquet RS, et al. Long-distance pollen flow assessment through evaluation of pollinator foraging range suggests transgene escape distances. *Proc Natl Acad Sci.* 2008;105(36):13456–61.
- Barlow SE, O'Neill MA, Pavlik BM. A prototype RFID tag for detecting bumblebee visitations within fragmented landscapes. *J Biol Eng.* 2019;13:1–6.
- Maggiara R, et al. An innovative harmonic radar to track flying insects: the case of *Vespa velutina*. *Sci Rep.* 2019;9(1):11964.
- Batsleer F, et al. The neglected impact of tracking devices on terrestrial arthropods. *Method Ecol Evol.* 2020;11(3):350–61.
- BENDER SFA, et al. Tracking honey bees using lidar (light detection and ranging) technology. Sandia National Lab(SNL-NM): Albuquerque; 2003.
- Guan Z, et al. Insect monitoring with fluorescence lidar techniques: Field experiments. *Appl Opt.* 2010;49(29):1–11.
- Månefjord H, et al. 3D-printed fluorescence hyperspectral lidar for monitoring tagged insects. *IEEE J Sel Top Quant Electr.* 2022;28(5):1–9.
- Aidoo K, Kwapong RC, Karikari IA. Stingless bees in Ghana. *Bees Dev J.* 2011;100:10–1.

54. Mathiasson, M.E., Early colony development of an equatorial afrotropical stingless bee (*Hypotrigona* sp.) In a new habitat. *J Young Investig.* 2015. 29.
55. Wang X, et al. Drone-based area scanning of vegetation fluorescence height profiles using a miniaturized hyperspectral lidar system. *Appl Phys B.* 2018. <https://doi.org/10.1007/s00340-018-7078-7>.
56. Zhao G, et al. Inelastic hyperspectral lidar for profiling aquatic ecosystems. *Laser Photonics Rev.* 2016;10(5):807–13.
57. Boateng R, et al. Remote vegetation diagnostics in Ghana with a hyperspectral fluorescence lidar. *IEEE J Sel Top Quant Electron.* 2023;29:1–7.
58. Hampus Månefjord LM, Salvador J, Runemark A, Kirkeby C, Brydegaard M. Low-cost and lightweight hyperspectral lidar for mapping vegetation fluorescence. In: Sullivan JT, Leblanc T, Tucker S, Demoz B, Eloranta E, Hostetler C, Ishii S, Mona L, Moshary F, Papayannis A, Rupavatharam K, editors. *EPJ web of conferences.* Cham: Springer International Publishing; 2022.
59. Brydegaard M, et al. The scheidpflug lidar method. in lidar remote sensing for environmental monitoring 2017. *Int Soc Opt Photon.* 2017;10406:104–20.
60. Mei L, Guan P. Development of an atmospheric polarization scheidpflug lidar system based on a time-division multiplexing scheme. *Opt Lett.* 2017;42(18):3562–5.
61. Mei L, Brydegaard M. Continuous-wave differential absorption lidar. *Laser Photonics Rev.* 2015;9(6):629–36.
62. Malmqvist E. From fauna to flames: remote sensing with scheidpflug lidar. Lund: Lund University; 2019.
63. Müller L, et al. Remote nanoscopy with infrared elastic hyperspectral lidar. *Adv Sci.* 2023;10(15):2207110.
64. Høye G, Løke T, Fridman A. Method for quantifying image quality in push-broom hyperspectral cameras. *Opt Engin.* 2015. <https://doi.org/10.1117/1.OE.54.5.053102>.
65. Malmqvist E, et al. Effective parameterization of laser radar observations of atmospheric fauna. *IEEE J Sel Top Quantum Electron.* 2015;22(3):327–34.
66. Taylor, G., R. Bomphrey, and J't Hoen. Insect flight dynamics and control. In: 44th AIAA aerospace sciences meeting and exhibit. 2006.
67. Naranjo SE. Influence of two mass-marking techniques on survival and flight behavior of *diabrotica virgifera virgifera* (coleoptera: chrysomelidae). *J Econ Entomol.* 1990;83(4):1360–4.
68. Daniel Kissling W, Pattermore DE, Hagen M. Challenges and prospects in the telemetry of insects. *Biol Rev.* 2014;89(3):511–30.
69. Boateng R, et al. Mapping of algae on walls with a 3d printed hyperspectral fluorescence lidar. in laser science. Washington DC: Optica Publishing Group; 2023.
70. Karikari AS, et al. 2012. What are the bees collecting?: case study of stingless bees in the central region of Ghana. In: Third international scientific symposium* Agrosym Jahorina.
71. Kiatoko N, et al. African endemic stingless bees as an efficient alternative pollinator to honey bees in greenhouse cucumber (*Cucumis sativus* L.). *J Apic Res.* 2021;62:1–13.
72. Willmer P, Bataw A, Hughes J. The superiority of bumblebees to honeybees as pollinators: insect visits to raspberry flowers. *Ecol Entomol.* 1994;19(3):271–84.

Publisher's Note

Springer Nature remains neutral with regard to jurisdictional claims in published maps and institutional affiliations.